Articles

Epitaxial Manganese Oxide Thin Films with Connected Porosity: Topotactic Induction of Crystallographic Pore Alignment

Eric S. Toberer,[†] Madeleine Grossman, Thomas Schladt, Frederick F. Lange, and Ram Seshadri*

Materials Department and Materials Research Laboratory, University of California, Santa Barbara, California 93106

Epitaxial thin films of $ZnMn_2O_4$, grown from an aqueous solution on (100) and (111) spinel $MgAl_2O_4$ substrates, have been topotactically reduced and leached to produce epitaxial rock salt MnO on the same substrates. The volume change accompanying the conversion of $ZnMn_2O_4$ to 2MnO associated with a loss of Zn and O_2 manifests as a network of interconnected, 50−100 nm pores. The topotactic nature of the transformation ensures that the pores are crystallographically aligned with the substrate: on the (100) $MgAl_2O_4$ substrate, pores with rectangular cross-sections are aligned parallel to the surface normal. On the (111) $MgAl_2O_4$ substrate, the pores are aligned at constant, fixed angles with respect to the substrate normal.

1. Introduction

Among the numerous techniques that exist for the preparation of porous materials, some of the most useful rely on spontaneous phase separation through chemical reaction or through spinodal processes. For example, Raney nickel skeletons are formed upon dissolution of a soluble metal (Al) from binary Al−Ni alloys and intermetallics.[1] When such dissolution processes are applied to the Au−Ag system, nanoporous Au is obtained.[2] Porous Vycor glass is formed through the spinodal decomposition of a borosilicate melt into borate-rich and -poor regions in the glass. The borate-rich regions can be acid-leached, resulting in porous glass.[3] Similarly, Millipore filter membranes are frequently manufactured by employing microscopic phase separation in solution processed polymer thin films.

Spontaneous routes to pore formation have been employed in inorganic materials and ceramics. Gorte and Vohs have described a number of spontaneous routes for porous

* Corresponding author. E-mail: seshadri@mrl.ucsb.edu.
† Current address: Materials Science, California Institute of Technology, Pasadena, CA 91125.

(1) Raney, M. Method of producing finely divided nickel, U.S. Patent 1628190, 1927.
(2) Erlebacher, J.; Aziz, M.; Karma, A.; Dimitrov, N.; Sieradzki, K. *Nature* **2001**, *410*, 450.
(3) Levitz, P.; Ehret, G.; Sinha, S. K.; Drake, J. M. *J. Chem. Phys.* **1991**, *95*, 6151.

electrode materials in solid oxide fuel cells.[4] Suzuki et al. have described the preparation of monoliths with directional porosity through the controlled cooling of eutectics,[5] the preparation of porous CaZrO$_3$/MgO composites by the reactive sintering of dolomite with ZrO$_2$,[6] and the preparation of porous CaZrO$_3$/MgAl$_2$O$_4$ composites by the reactive sintering of dolomite, zirconia, and alumina.[7] Singh et al. have shown that porous films of TiO$_2$ can be prepared by exploiting Bénard−Marangoni convection.[8]

In our work, we have employed controlled solid state and solid−gas reactions to prepare two-phase composites wherein each component has distinct reactivity. The removal of one of the phases results in the other phase being rendered porous. For example, NiO/ZnO composites can be prepared by the decomposition of precursors containing both cations. ZnO can be removed to yield porous NiO, which can further be conformally reduced to porous Ni.[9] Variations on this theme allow a number of different functional inorganic materials to be prepared as monoliths with connected pores.[10−12] We have extended these techniques to the preparation of hierarchically porous materials.[13−16] For this, we employ successive stages of leaching: a phase from a biphasic composite and, then, of components from the ensuing pure porous material. The second stage in the process typically involves the volatilization and removal of species. In both stages, the accompanying volume losses manifest in the monolith as connected pores with different characteristic dimensions. These methods have been reviewed.[17]

In the formation of porous MnO by the vapor-phase leaching of Zn and O from ZnMn$_2$O$_4$,[13,14] we have been struck by the crystallographic alignment of the resulting mesopores, which we believe to arise from topotactic processes. It is known that Mn$_3$O$_4$ reduces to MnO topotactically in epitaxial thin film architectures.[18] Here, we attempt to better understand and control the pore formation process by carrying them out on epitaxial thin films. We employ a low temperature aqueous method to epitaxially grow hetærolite ZnMn$_2$O$_4$, a compound whose structure is closely related to spinel, on lattice-matched spinel MgAl$_2$O$_4$ substrates. Subsequent reduction and vapor-phase leaching of these films leaves behind a single-crystal film of MnO on the MgAl$_2$O$_4$ substrate. The reduction replicates the behavior found for polycrystalline ZnMn$_2$O$_4$ in the bulk, viz. volume loss associated with reduction, and with leaching of Zn in the vapor phase. It produces a MnO film containing interconnected mesopores that share a common orientation relative to the single-crystal film and substrate.

Other systems with pores penetrating through single crystals include certain bioskeletons[19] and their synthetic mimics[20,21] and the products of electrochemical etching of silicon wafers.[22] Turbine blades in many modern gas turbine engines are single-crystal metals or alloys with holes drilled though them for thermal management.

The motivation for using low temperature aqueous methods for the starting thin films is derived from their proven versatility for growing oxides epitaxially on oxide single-crystal substrates. Properly carried out, nucleation occurs heterogeneously on the substrate, which results in dense epitaxial films with a controlled thickness. Many perovskite materials have been grown on single-crystal SrTiO$_3$ substrates, including BaTiO$_3$, PbTiO$_3$, KTaO$_3$, and KNbO$_3$.[23−27] The (111) surface of MgAl$_2$O$_4$ has recently been used to template epitaxial films of ZnO in water.[28,29] Undoped and Mn-doped ZnGa$_2$O$_4$ thin films have been epitaxially stabilized from aqueous solution on MgAl$_2$O$_4$.[30]

2. Experimental Procedures

ZnMn$_2$O$_4$ films were prepared on MgAl$_2$O$_4$ substrates by low temperature aqueous growth at 150 °C. MgAl$_2$O$_4$ substrates with (100) and (111) surfaces were cleaned by rinsing with ethanol and acetone and heating at 700 °C for 2 h. Teflon-lined 23 cm^3 hydrothermal bombs (Parr) were filled with 10 cm^3 of a 0.05 M metal acetate solution [1:2 Zn(CH$_3$COO)$_2$/Mn(CH$_3$COO)$_2$]. The pH of the solution was adjusted to stated values with concentrated acetic acid or ammonia. Films were grown by suspending the substrates polished side down in the solution and heating to 150 °C for 2−72 h. Growing films on the undersides of substrates helped avoid homogeneously precipitated particles from sedimenting onto the film. Thicker films were produced by repeating the growth procedure 4 times with fresh solutions. The yield of ZnMn$_2$O$_4$ powders as a function of pH, precursor concentration, temperature, and ramp rate was also investigated. Following growth, some of the films were annealed at 900 °C for 2 h. All films were reduced to MnO by heating in a flowing 5% H$_2$−N$_2$ atmosphere at temperatures ranging from 450 to 650 °C for 1−4 h.

(4) Gorte, R.; Vohs, J. *J. Catal.* **2003**, *216*, 477.
(5) Suzuki, Y.; Yamada, T.; Sakakibara, S.; Ohji, T. *Ceram. Eng. Sci. Proc.* **2000**, *21*, 19.
(6) Suzuki, Y.; Morgan, P. E. D.; Ohji, T. *J. Am. Ceram. Soc.* **2003**, *86*, 2091.
(7) Suzuki, Y.; Kondo, N.; Ohji, T. *J. Am. Ceram. Soc.* **2003**, *86*, 1128.
(8) Singh, R. S.; Grimes, C. A.; Dickey, E. C. *Mater. Res. Innov.* **2001**, *5*, 178.
(9) Rajamathi, M.; Thimmaiah, S.; Morgan, P. E. D.; Seshadri, R. *J. Mater. Chem.* **2001**, *11*, 2489.
(10) Panda, M.; Rajamathi, M.; Seshadri, R. *Chem. Mater.* **2002**, *14*, 4762.
(11) Toberer, E. S.; Weaver, J. C.; Ramesha, K.; Seshadri, R. *Chem. Mater.* **2004**, *16*, 2194.
(12) Toberer, E. S.; Joshi, A.; Seshadri, R. *Chem. Mater.* **2005**, *17*, 2142.
(13) Toberer, E. S.; Seshadri, R. *Adv. Mater.* **2005**, *17*, 2244.
(14) Toberer, E. S.; Löfvander, J. P.; Seshadri, R. *Chem. Mater.* **2006**, *18*, 1047.
(15) Toberer, E. S.; Schladt, T.; Seshadri, R. *J. Am. Chem. Soc.* **2006**, *128*, 1462.
(16) Toberer, E. S.; Epping, J.-D.; Chmelka, B. F.; Seshadri, R. *Chem. Mater.* **2006**, *18*, 6435.
(17) Toberer, E. S.; Seshadri, R. *J. Chem. Soc., Chem. Commun.* **2006**, 3159.
(18) Caslavska, V.; Roy, R. *J. Appl. Phys.* **1970**, *41*, 825.

(19) Donnay, G.; Pawson, D. L. *Science* **1969**, *166*, 1147.
(20) Park, R. J.; Meldrum, F. C. *J. Mater. Chem.* **2004**, *14*, 2291.
(21) Aizenberg, J.; Muller, D. A.; Grazul, J. L.; Hamann, D. R. *Science* **2003**, *299*, 1205.
(22) Lin, V. S.-Y.; Motesharei, K.; Dancil, K.-P. S.; Sailor, M. J.; Ghadiri, M. R. *Science* **1997**, *31*, 840.
(23) Chien, A. T.; Speck, J. S.; Lange, F. F.; Daykin, A. C.; Levi, C. G. *J. Mater. Res.* **1995**, *10*, 1784.
(24) Chien, A. T.; Sachleben, J.; Kim, J. H.; Speck, J. F.; Lange, F. F. *J. Mater. Res.* **1999**, *14*, 3303.
(25) Ahn, S. H.; Jung, W. W.; Choi, S. K. *Appl. Phys. Lett.* **2005**, *86*, 172901.
(26) Goh, G. K. L.; Levi, C. G.; Lange, F. F. *J. Mater. Res.* **2002**, *17*, 2852.
(27) Suchanek, W. *Chem. Mater.* **2004**, *16*, 1083.
(28) Andeen, D.; Loeffler, L. L.; Padture, N.; Lange, F. F. *J. Cryst. Growth* **2003**, *259*, 103.
(29) Andeen, D.; Kim, J. H.; Lange, F. F.; Goh, G. K.; Tripathy, S. *Adv. Funct. Mater.* **2006**, *16*, 799.
(30) Loeffler, L.; Lange, F. F. *J. Mater. Res.* **2002**, *19*, 902.

Phase identification of the precipitated powders was determined by X-ray diffraction and Rietveld refinement (Philips X'PERT MPD). The thin films were characterized by X-ray diffraction $\theta-2\theta$ scans, ω rocking curves, and ϕ scans (PANalytical MRD PRO). Thin film morphology and composition were characterized by scanning electron microscopy and energy-dispersive X-ray analysis on an FEI XL40 Sirion system.

3. Results and Discussion

3.1. Powders. To develop an understanding of the phase space for $ZnMn_2O_4$ film growth, hydrothermal treatments of aqueous solutions containing zinc and manganese ions were carried out at different conditions of pH, temperature, and time. At 150 °C, no precipitation occurred when the pH was equal to 4.5. With an increasing pH, the $ZnMn_2O_4$ powder begins to precipitate, and by pH = 5.5, a 30% yield relative to the starting amounts of the cations is obtained. Above pH = 8.5, manganese hydroxide precipitation occurs at room temperature. Using powder X-ray diffraction of the precipitate resulting from treatment of the starting acetates at pH = 6.5 and at 150 °C, the powder is entirely $ZnMn_2O_4$. Rietveld refinement using the XND code[31] in the $I4_1/amd$ structure gave a unit cell volume of 301.51(8) $Å^3$, which is slightly smaller than the reported value of 302.48 $Å^3$.[32] EDX measurements of the powder give a Zn/Mn ratio close to 1:2.1, suggesting some Mn^{2+} in the A-site. The results are in agreement with the Pourbaix solubility diagram,[33] recognizing that at higher temperatures, the diagram generally shifts toward lower pH values. It should be noted that we are starting with divalent cations and forming a compound with Mn^{3+}. The in situ oxidation of Mn^{2+} to Mn^{3+} is believed to be caused by the ambient oxygen.[34]

3.2. Thin Films. Thin film XRD confirmed that the $ZnMn_2O_4$ thin films were epitaxial with the spinel single-crystal substrates. While approximately isostructural with $MgAl_2O_4$ spinel, the conventional $ZnMn_2O_4$ unit cell is rotated by 45° about the c-axis relative to the $MgAl_2O_4$ unit cell. In addition, the a and b cell parameters are divided by $\sqrt{2}$, and the c-axis is slightly elongated due to Jahn−Teller distorted Mn^{3+} octahedra ($ZnMn_2O_4$: $I4_1/amd$ with $a = 5.720$ Å and $c = 9.245$ Å; $MgAl_2O_4$: $Fd\bar{3}m$ with $a = 8.0831$ Å). Figure 1 shows the two unit cells, with the $ZnMn_2O_4$ cell rotated to illustrate the relation between the two different crystal structures. Panels c−f of Figure 1 show several sets of substrate and film Bragg planes that are nearly parallel and are used to understand the thin film XRD data.

Observations of the film at an early stage of growth showed that $ZnMn_2O_4$ nucleated on the substrates to form isolated pyramids. As the pyramids grow larger, they coalesce to form a continuous film. This is seen in the SEM image in Figure 2 of a continuous $ZnMn_2O_4$ film grown on (100) $MgAl_2O_4$. The conditions for film growth were pH =
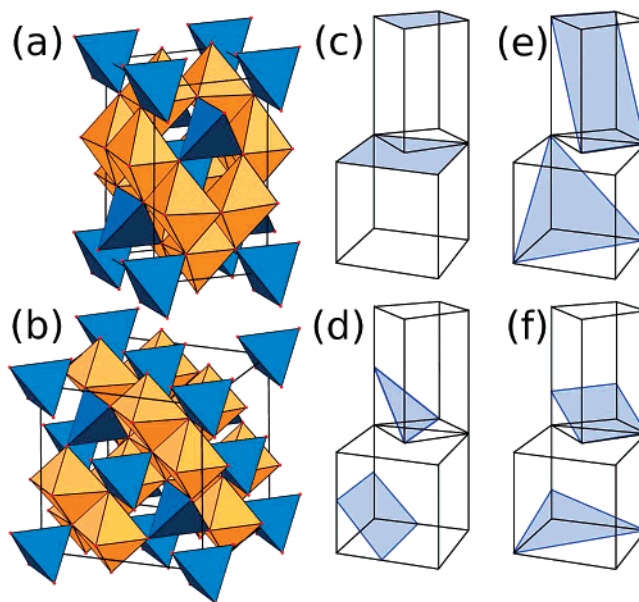
(31) Bérar, J.-F.; Garnier, P. *NIST Special Publication*; NIST: Washington, DC, 1992; Vol. 846, p 212; http://www.ccp14.ac.uk.
(32) Åsbrink, S.; Waœckowska, A.; Gerward, L.; Olsen, J. S.; Talik, E. *Phys. Rev. B* **1999**, *60*, 12651.
(33) Pourbaix, M. *Atlas of Electrochemical Equilibria in Aqueous Solutions*; Pergamon Press: Oxford, 1966.
(34) Makovec, D.; Drofenik, M.; Žnidaršiè, A. *J. Am. Ceram. Soc.* **1999**, *82*, 1113.

Figure 1. (a) Unit cell of hetærolite (tetragonally distorted spinel) $ZnMn_2O_4$ and (b) unit cell of the cubic $MgAl_2O_4$ spinel substrate, showing Zn- or Mg-centered tetrahedra in orange and Mn- or Al-centered octahedra in blue. When the unit cells of the film (f) and substrate (sub) are oriented as displayed, the following sets of Bragg planes are approximately coplanar: (c) $(001)_f$ and $(001)_{sub}$, (d) $(112)_f$ and $(202)_{sub}$, (e) $(101)_f$ and $(111)_{sub}$, and (f) $(103)_f$ and $(113)_{sub}$.
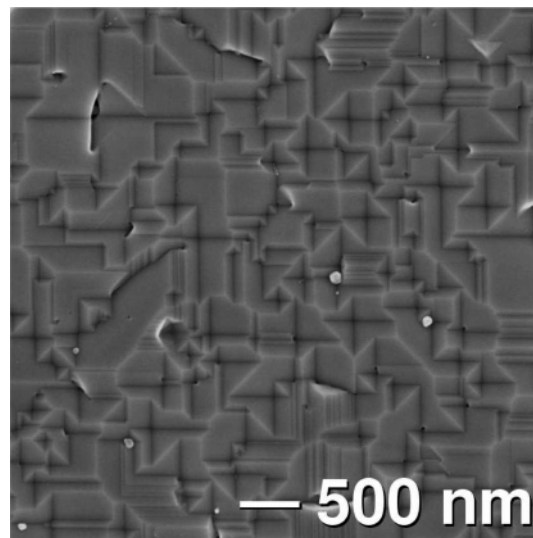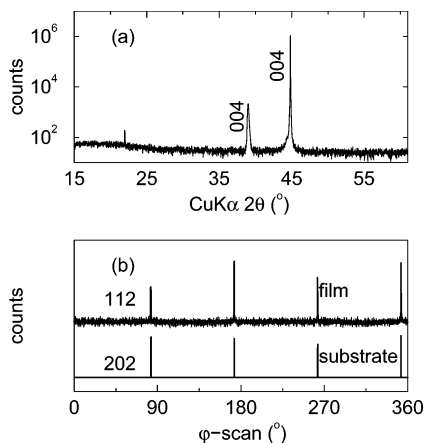

Figure 2. Scanning electron micrograph of the surface of a $ZnMn_2O_4$ film grown on a (100) $MgAl_2O_4$ substrate. The initially nucleated grains are square-pyramidal in shape, and these coalesce to give a continuous film. Note that all grains have the same relative orientation.

6.5 at 150 °C for 18 h. Films 250 nm thick form after growths of only 1 h, while films with thicknesses of 2 μm formed after 3 days. EDX measurements of the film elemental composition confirmed the 1:2 Zn/Mn stoichiometry expected for $ZnMn_2O_4$. The sharp edges of the coalesced grains run either top to bottom or left to right in the image, suggesting that the grains and hence the film is strongly correlated in-plane with the substrate.

Thin film XRD patterns are shown for films grown on (100) oriented $MgAl_2O_4$ in Figure 3a,b. The $\theta-2\theta$ scans only show the (004) $ZnMn_2O_4$ and substrate reflections, indicating that the c-axis of the film grows out parallel to the c-axis of the spinel substrate. With the out-of-plane orientation

Figure 3. (a) $\theta-2\theta$ scan and (b) selected ϕ scans of the ZnMn$_2$O$_4$ film grown on a (100) MgAl$_2$O$_4$ substrate. Together, the data indicate that the ZnMn$_2$O$_4$ film is an epitaxial continuation of the underlying spinel lattice.
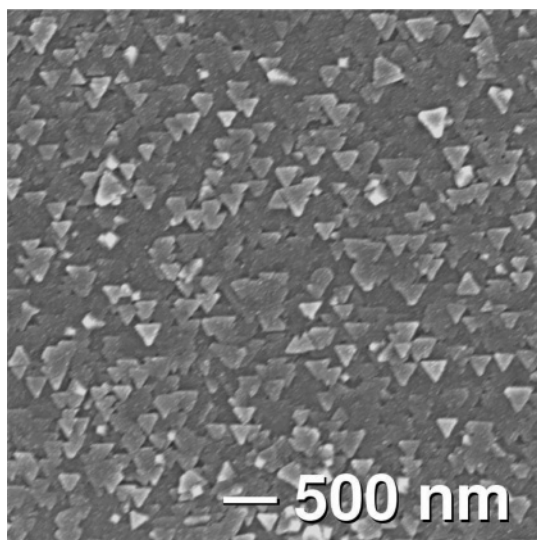

Figure 4. Scanning electron micrograph of the surface of a ZnMn$_2$O$_4$ thin film grown on a (111) MgAl$_2$O$_4$ substrate. Initial grains are triangular, and these coalesce to give a continuous film. Note that all grains have the same relative orientation.

established, the in-plane orientation is resolved with off-axis ϕ scans (Figure 3b). The substrate (202) and film (112) reflections are superimposed with ϕ, indicating that the ZnMn$_2$O$_4$ cell is a continuation of the underlying lattice. The relationship between (202)$_{sub}$ and (112)$_f$ reflections can been seen in the schematic in Figure 1d. The preferential orientation of the long c-axis out-of-plane arises from the low mismatch between the (001) plane with the substrate (0.07% mismatch). The low mismatch is reflected in the small ω rocking curve widths obtained for films grown on the (100) substrates. On-axis (004) full width at half-maximum (fwhm) values of 0.05° and off-axis (112) fwhm values of 0.15° were found.

Films grown on the (111) MgAl$_2$O$_4$ displayed a similar growth behavior and formed continuous films with triangular grains (Figure 4). Once again, all the grain edges are aligned in one of three directions, suggesting in-plane correlations. Figure 5a shows $\theta-2\theta$ XRD patterns of such films: ZnMn$_2$O$_4$ (101) reflections are the only film peaks present, indicating an out-of-plane orientation, given that the (101) planes of ZnMn$_2$O$_4$ are nearly parallel to the (111) planes
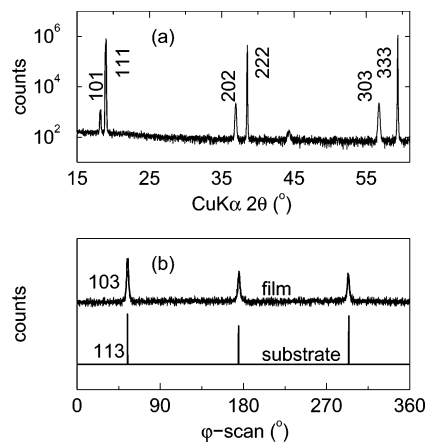

Figure 5. (a) $\theta-2\theta$ scan and (b) selected ϕ scans of the ZnMn$_2$O$_4$ film grown on a (111) MgAl$_2$O$_4$ substrate. Data suggest that the ZnMn$_2$O$_4$ film is an epitaxial continuation of the underlying spinel lattice.

of the substrate spinel. Figure 1e shows the (101)$_f$ and (111)$_{sub}$ planes as approximately coplanar (planes are rotated by 3.86° about the substrate [110] direction). Off-axis ϕ scans in Figure 5b show (103)$_f$ and (113)$_{sub}$ reflections every 120° and are superimposed with respect to ϕ. The schematic in Figure 1f shows (103)$_f$ and (113)$_{sub}$ planes with the unit cells oriented so that these ϕ scans would be superimposed. As in the (100) MgAl$_2$O$_4$ substrates, films grow on the (111) substrates as a continuation of the underlying spinel lattice. The lattice mismatch for ZnMn$_2$O$_4$ grown on the (111) substrates is much larger than on the (100) substrates as the orientation brings the long c-axis into the plane. The (111) face of MgAl$_2$O$_4$ is formed of equilateral triangles, whereas the (101) ZnMn$_2$O$_4$ face is composed of isosceles triangles, leading to a 11 and 0.07% misfit between the film and the substrate. Despite the large misfit, the epitaxial relationship with the substrate is maintained. For films on the (111) substrates, ω rocking curves are noticeably broader than films on (100) substrates, with on-axis (202) reflections giving a 0.75° fwhm and off-axis (103) reflections a 1.15° fwhm.

3.3. Reduction and Leaching of ZnMn$_2$O$_4$ Films to ZnO. The reduction of ZnMn$_2$O$_4$ to 2MnO, with Zn and O being carried away in the reduction stream, is accompanied by a 42% decrease in volume. Our previous work on polycrystalline materials[13,14] had suggested that the conversion takes place topotactically resulting in crystals of MnO that contain connected, percolating pores. In the current experiments, where the crystallography of all phases is well-known, the relative orientation can be related to that of the MgAl$_2$O$_4$ spinel substrate. Here, we have a way of externally constraining the manner in which pores form since their geometries will be dictated by their relative orientation with the spinel MgAl$_2$O$_4$ substrate.

Figure 6 shows a ZnMn$_2$O$_4$ film grown on a (100) MgAl$_2$O$_4$ substrate after its reduction to MnO. The film is perforated with aligned pores identical to those found in the bulk, with rectangular walls comprising (100) planes. The pores are negative crystals relative to the structure of MnO, meaning that they have holes bounded by crystallographic faces. Typical pore sizes are between 50 and 100 nm. The cross-section shows that the pores are aligned in the [100] directions.
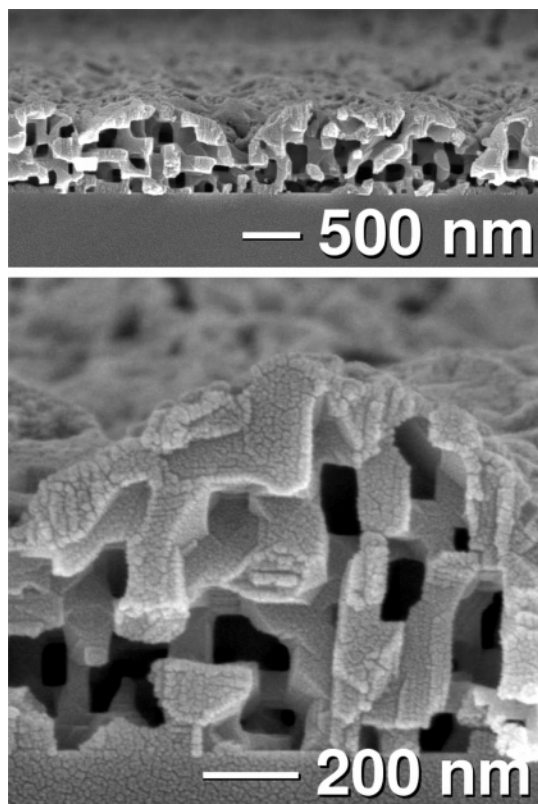
Epitaxial Mn Oxide Thin Films with Connected Porosity

Chem. Mater., Vol. 19, No. 20, 2007 4837

Figure 6. SEM cross-sections of the MnO film formed on the (100) MgAl$_2$O$_4$ substrate by reduction and vapor-phase leaching of a ZnMn$_2$O$_4$ thin film. The film is entirely perforated with connected mesopores. Note that the pores are aligned flat with the substrate.

Figure 7. XRD reveals the topotactic nature of the reduction to MnO. (a) $\theta-2\theta$ scan showing out-of-plane orientation and (b) ϕ scans showing in-plane orientation of the MnO film on (100) MgAl$_2$O$_4$.

Figure 8. SEM cross-sections of the MnO film formed on the (111) MgAl$_2$O$_4$ substrate following reduction and vapor-phase leaching of an epitaxial ZnMn$_2$O$_4$ thin film. The film is entirely perforated with connected mesopores. Note that the pores are aligned at an angle of 54.74° with respect to the substrate.

The unit cell edge of MnO (cubic, $a = 4.46$ Å) is slightly larger than half the spinel unit cell edge (cubic, $a = 8.0831$ Å), which means that cube-on-cube epitaxy of MnO on MgAl$_2$O$_4$ is possible, albeit with a lattice mismatch near 10%. X-ray diffraction studies were performed to understand the crystallographic relationship associated with the spinel to rock salt transformation and to correlate crystallography with the resulting pore morphology. After reduction, $\theta-2\theta$ XRD scans showed only (200) MnO reflections for the (100) substrates (Figure 7a). The usual dominant (111) reflection of MnO is strongly suppressed, even with diffraction intensities plotted on a log scale. In-plane orientation of the films following reduction was observed with ϕ scans and is shown in Figure 7b. The superposition with ϕ between the substrate and the film reflections indicates that the in-plane axes are parallel across the interface.

For ZnMn$_2$O$_4$ films grown on the (111) substrates, reduction produced rectangular pores 30−50 nm in width/height as shown in Figure 8. The pores are aligned throughout the entire film, with [100] substrate and film directions. In the cross-section, the pore walls appear rotated with respect to the substrate, unlike the pores formed in the reduced films on the (100) substrates, which are parallel with the surface. The rotation angle is the angle between the (100) planes and the (111) planes, namely, 54.74°. As shown in Figure 9, XRD patterns show only (111) MnO reflections after reduction on the (111) substrate, indicating that the out-of-plane orientation was retained through the reductive transformation. The in-plane orientation is also conserved,
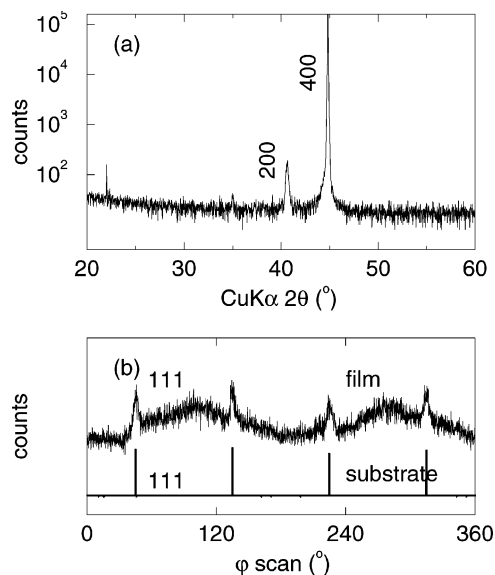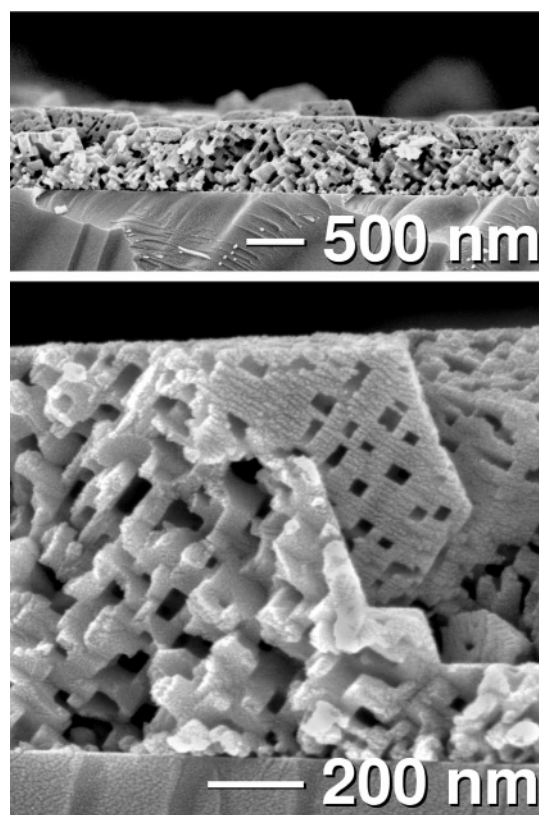
as seen in the ϕ scan (Figure 9b), with broad (100) peaks every 120° and aligned with the substrate (400) peaks.

For both (100) and (111) substrate orientations, the lattice mismatch between MnO and spinel is quite large (near 10%), leading to a broadening of the ω rocking curves and ϕ scans. For MnO on the (100) substrate, the ω rocking curve fwhm was 5° for the (200) reflection. MnO on the (111) substrate
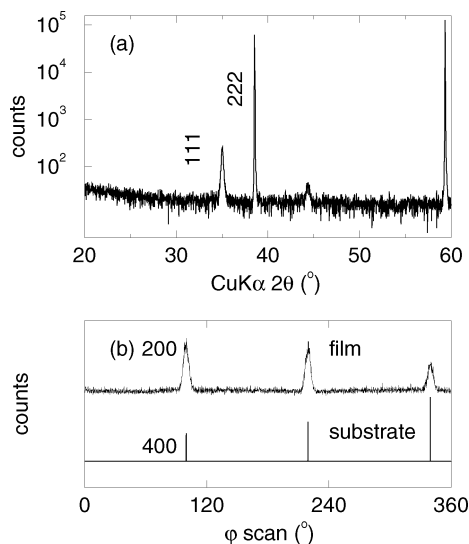
Figure 9. XRD reveals the topotactic nature of the reduction to MnO. (a) $\theta-2\theta$ scan showing out-of-plane orientation and (b) ϕ scans showing in-plane orientation of the MnO film on (111) MgAl$_2$O$_4$.

had a ω rocking curve fwhm of 7 and 5° for the (111) and (200) reflections, respectively. The reflections indicate that the in-plane axes are parallel across the interface.

The relationship between crystal orientation and pore architecture in these thin films is identical to that previously found for the corresponding polycrystalline material.[13,14] The pores in MnO are oriented along the [100] directions with walls composed of (100) planes, which are the stable, charge-neutral planes for the rock salt MnO structure. For films grown on the (100) substrate, the pores are aligned parallel to the substrate−film interface, and for (111) films, the pores are oriented at an angle of 54.7° from the substrate. As the entire film is an epitaxial continuation of the single-crystal substrate, the pores are themselves macroscopically aligned along the degenerate crystallographic directions.

In summary, a spontaneous method to pattern mesopores at macroscopic length scales has been developed. Films of ZnMn$_2$O$_4$ have been epitaxially grown via low temperature solution methods on single-crystal substrates. Subsequent reduction and vapor-phase leaching at high temperatures convert these films to MnO in a topotactic manner. The volume loss inherent in these transformations produces aligned pores that appear as negative crystals across the entire film. The pores are approximately 50−100 nm in width on the (100) substrate and approximately 30−50 nm in width on the (111) substrate.